RSC Advances

PAPER

View Article Online
View Journal | View Issue

Cite this: *RSC Adv.*, 2024, **14**, 16501

Gd_2O_3-modulated borate glass for the enhancement of near-infrared emission *via* energy transfer from Gd^{3+} to Nd^{3+}

I. Ullah, [a] C. S. Sarumaha,[cd] A. Angnanon,[e] I. Khan, [a] M. Shoaib,[b] S. A. Khattak, [a] S. Mukamil,[a] S. Kothan,[e] S. K. Shah, [a] S. M. Wabaidur,[f] G. Rooh[a] and J. Kaewkhao*[cd]

Received 4th March 2024
Accepted 30th April 2024

DOI: 10.1039/d4ra01682c

rsc.li/rsc-advances

$(Li_2O)_{0.20}(SrO)_{0.30}(Nd_2O_3)_{0.01}(B_2O_3)_{0.49-x}(Gd_2O_3)_x$, where x = 0, 3, 5, 7, and 10 mol%, glass was melt-quenched to test it as a laser source in the near-infrared (NIR) region. The structural modification, absorption spectra, Judd–Ofelt (J–O) parameters, luminescence spectra, radiative laser parameters, lifetimes, XRD, and FTIR spectra were studied. Luminescence spectra excited at λ_{exc} = 584 nm revealed the highest intensity peak at 1073 nm due to the transition of $^4F_{3/2} \rightarrow {}^4I_{11/2}$. An important phenomenon of concentration quenching was observed and optimized luminescence was achieved with the sample having the concentration x = 07 mol%. The lifetimes of the donor and acceptor and energy transfer from gadolinium to neodymium were obtained from the luminescence decay kinetics. The findings show that Nd-doped Gd_2O_3-modified glass materials have potential as NIR laser sources.

1. Introduction

There has been an intense quest for new materials to work as near-infrared (NIR) light sources with superior optical and luminescence properties to fulfill the required demands of several photonic devices such as optical amplification, infrared laser, and optical communication.[1,2] Among these optical devices, near-infrared solid-state lasers are attracting attention for their versatility.[3–5] Considering the excellent spectral characteristics of RE^{3+}, RE^{3+}-doped inorganic materials are attracting great interest as potential lasing compounds.[6,7] With this in view, Nd-added compounds are considered promising because of their significant NIR luminescence.[8,9] Many glasses have demonstrated to be better host matrices than single crystals for solid-state lasers.[3] Therefore, various Nd-doped inorganic oxide glasses such as silicates,[10] phosphates,[11] tellurites,[12] and borates[13] have been developed. It has been reported in different studies that the doping of Nd into various hosts can improve NIR radiative properties of the glasses. However, the improvement in such radiative properties varies across the host matrices. Therefore, the quest for a promising host with the Nd dopant for NIR emission is still ongoing. Although, borate glasses are structurally more complex compared to silicate and phosphate glasses, they possess high transparency, a higher refractive index, and greater REIs solubility.[14] Specific glasses require particular properties; for instance, for broadband emission glasses, several emission centers in the host matrix are required that can be obtained through searching a matrix having different local surroundings for activators. However, because of the limited mixing in hosts, the agglomeration of Nd_2O_3 occurs.[15] Thus, since Nd^{3+} possesses comparatively narrow absorption bands, most of the broadband excitation does not take place.[15] A solution to this problem is to co-dope the glass with Nd^{3+} and another suitable sensitizer/donor that may sensitize Nd^{3+} *via* energy transfer (ET). Using this sensitization strategy, the desired optical amplification may be obtained. Previously, several glasses codoped with rare earth and their light-emitting properties have been reported. The ET phenomenon, which takes place non-radiatively, between the dopants in the Nd–Gd-codoped borate matrix was studied by C. R. Kesavulu *et al.*,[16] where these glass systems were suggested to be efficient in NIR lasers operating at λ = 1059 nm. I. Ullah *et al.*[17] studied the intense emission that arose because of ET from gadolinium ions to Nd^{3+} caused by UV excitation in borate systems. The luminescence and Judd–Ofelt (J–O) analyses, and lifetime studies have demonstrated that these glasses are promising for NIR laser devices having an appropriate energy-gain ratio and suitable lasing threshold. Acting as an efficient sensitizer/donor, gadolinium ions have exhibited intense UV

[a]*Department of Physics, Abdul Wali Khan University, Mardan, 23200, Pakistan*
[b]*School of Energy and Power Engineering, Jiangsu University, Zhenjiang 212013, Jiangsu, P. R. China*
[c]*Center of Excellence in Glass Technology and Materials Science (CEGM), Nakhon Pathom Rajabhat University, Nakhon Pathom, 73000, Thailand. E-mail: jakrapong@webmail.npru.ac.th*
[d]*Physics Program, Faculty of Science and Technology, Nakhon Pathom Rajabhat University, Nakhon Pathom, 73000, Thailand*
[e]*Center of Radiation Research and Medical Imaging, Department of Radiologic Technology, Faculty of Associated Medical Sciences, Chiang Mai University, Chiang Mai, 50200, Thailand*
[f]*Department of Chemistry, College of Science, King Saud University, Riyadh 11451, Saudi Arabia*

excitation because of $^{8}S_{7/2} \rightarrow {}^{6}I_{J}$ transitions.[18] Therefore, the spectroscopic and laser characteristics of neodymium in borate systems may be improved by Gd co-doping *via* ET from the sensitizer to the activator.

Here we aimed to get insights into the enhancement of the neodymium ions photoluminescence in LSBNd_*x*Gd glasses using Gd co-doping by calculating and analyzing the related radiative parameters required for laser applications.

2. Materials and methods

LSBNd_*x*Gd glasses, specifically $(Li_2O)_{0.20}(SrO)_{0.30}(B_2O_3)_{0.49-x}(Nd_2O_3)_{0.01}(Gd_2O_3)_x$ (where $x = 0$, 3, 5, 7, 10 mol%), were developed using $LiCO_3$, $MgCO_3$, H_3BO_3, Nd_2O_3, and Gd_2O_3 as precursor materials (procured from Sigma-Aldrich as 99.99% pure), which were weighed and homogeneously mixed in a porcelain crucible and then heated at 1100 °C for 4 h in a furnace at a rate of 10 °C min^{-1}. The melt was quenched on a steel mold. Annealing of the as-prepared glasses was carried out at 300 °C for 3 h to remove the potential thermal stresses. The prepared glass samples were denoted as LSBNd_0Gd, LSBNd_3Gd, LSBNd_5Gd, LSBNd_7Gd, and LSBNd_10Gd, corresponding to 0, 3, 5, 7, and 10 mol% Gd^{3+} concentrations, as shown in Fig. 1.

A densitometer (Diethelm Limited, HR-200) and Abbe refractometer (ATAGO) were used to measure the density (d) and refractive index (n) of the samples, respectively. XRD analysis was conducted using a Shimadzu XRD-6100 diffractometer with Cu Kα-radiation, 40 kV, and 30 mA power. The Agilent Cary 630 FTIR system was used to obtain the FTIR spectra. The absorption spectra were recorded by employing a Shimadzu 3600 UV-VIS-NIR spectrophotometer. The photoluminescence excitation and emission spectra and lifetime decay spectra were obtained using a Cary Eclipse fluorescence spectrophotometer (Agilent Technologies).

3. Results and discussion

3.1. XRD and FTIR features

The comprehensive absence of sharp diffraction peaks in the X-ray diffraction (XRD) patterns in Fig. 2 and characteristic broad humps at lower angles, notably around 28°, with an absence of well-defined sharp peaks was indicative of a disordered and random distribution of atoms in these materials, reinforcing the conclusion that the samples exhibited an amorphous phase.[19] This structural characteristic is crucial in understanding and assessing the unique properties and applications of amorphous materials in various fields, such as solid-state devices, LEDs, and lasers.

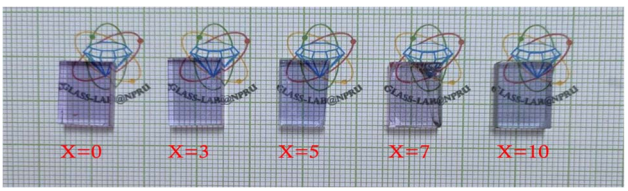

Fig. 1 Photos of the developed glasses with increasing Gd_2O_3 content (mol%) from left to right.

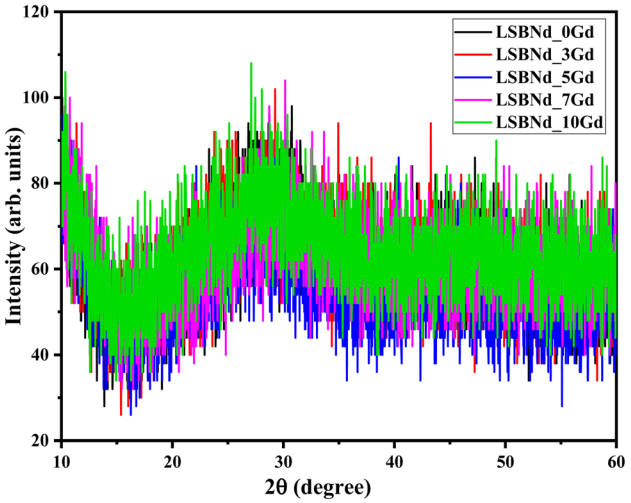

Fig. 2 XRD features of the LSBNd_*x*Gd glasses.

Fourier transform infrared spectroscopy (FTIR) can play a crucial role in the analysis of borate glasses, providing valuable insights into their molecular structure and vibrational characteristics. In the FTIR spectra of borate glasses, three distinct frequency regions are typically observed. The bands within the ranges of 1200–1450 cm^{-1} and 850–1200 cm^{-1} are associated with B–O stretching vibrations, specifically those of trigonal BO_3 units and tetrahedral BO_4 borate units, respectively.[20] Additionally, a peak around 700 cm^{-1} can be attributed to the bending vibrations of B–O linkages within the borate network. Further, in-depth analysis reveals that specific bands, such as those between 850–1168 cm^{-1} and 892–1195 cm^{-1}, represent the B–O stretching vibrations of tetrahedral BO_4 units. Notably, the band at approximately 1200 cm^{-1} is linked to the stretching vibrations of B–O bonds in $(BO_3)^-$ units, primarily involving the oxygen atoms that connect different groups. These band assignments are often derived from previous reports,[21] emphasizing the significance of FTIR in characterizing the structural features and bonding arrangements of borate glasses, thereby contributing to a comprehensive understanding of their properties. Here, the peak at 838 cm^{-1} was slightly shifted toward higher a wave number (840 cm^{-1}) with the increase in Gd_2O_3 content. This suggests that the introduction of Gd_2O_3 induced changes in the spectra of the samples, particularly in terms of peak positioning. This shift in peak position is indicative of structural alterations within the matrix. From the current discussion it is clear that structural modification indicated by the changes in physical parameters (density and molar volume) were also reflected in the FTIR spectra, *i.e.*, the slight redshift of the peak from 838 cm^{-1} to 840 cm^{-1} with increasing the Gd dopant from 0 to 7 mol%; whereby the vibrations modes become more stretched because of the increase in density and molar volume (Fig. 3).

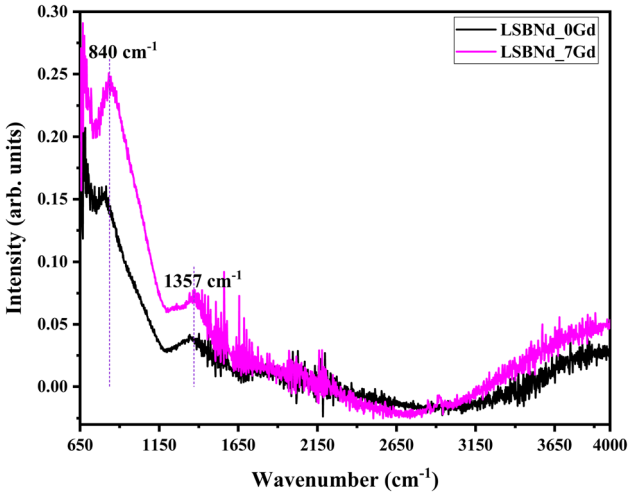

Fig. 3 FTIR bands features of LSBNd_*x*Gd glasses.

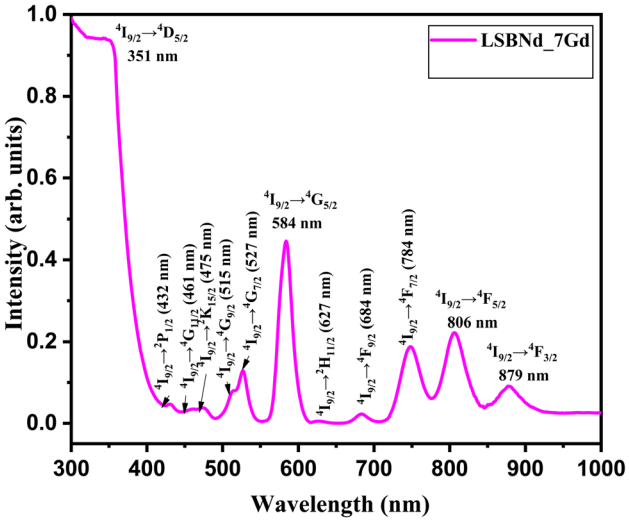

Fig. 5 Absorption spectrum of the LSBNd_7Gd glass.

3.2. Physical parameters

The essential parameters that determine the structural changes when the dopants are added are d, molar volume (V_m), and n.

Fig. 4 displays the variation in all these parameters for the LSBNd_*x*Gd glasses with varying the Gd_2O_3 concentration. Here, d was linearly elevated with the addition of Gd_2O_3 because of the substitution of BO_3 by BO_4 as well as due to the replacement of the lightweight B_2O_3 with a molecular weight of 69.622 g mol^{-1} by Gd_2O_3 with a heavier weight of 336.480 g mol^{-1}, making the glass more rigid. Hence, Gd_2O_3 doping modified the host matrix. Also, V_m was elevated with increasing the Gd_2O_3 content because the Gd^{3+} ions have a bigger ionic size than the boron and oxygen residing in the voids caused by bond rupture between boron and oxygen, while the number of Gd^{3+} per unit volume also rose.[22,23] Further, n was elevated with the addition of Gd_2O_3 as the speed of light in the materials was reduced.

3.3. Absorption spectra and Judd–Ofelt analysis

Fig. 5 displays the absorption spectrum of the LSBNd_7Gd sample showing multiple absorption peaks, characteristic of electronic transitions, positioned at 431, 462, 526, 582, 626, 682, 747, 806, and 876 nm, as per the analysis procedure reported in ref. 24 and 25.

3.3.1. Optical bandgap evaluation. The investigation into the bandgap properties of the samples revealed intriguing insights into their optical behavior. Tauc's approach[26] was employed to the absorption data to compute the optical bandgap, while Mott and Davis's method[27] was utilized for unlocking the direct or indirect transition. The computed indirect bandgap for the LSBNd_7Gd sample was 2.87 eV, as depicted in Fig. 6. Further exploration into the mechanisms underlying the bandgap modifications facilitated by additives like Gd_2O_3, holds promise for tailoring the optical properties of these materials to suit specific technological needs.

To determine the theoretical oscillator strength (f_{theo}) and intensity parameters, we performed Judd–Ofelt (J–O) analysis

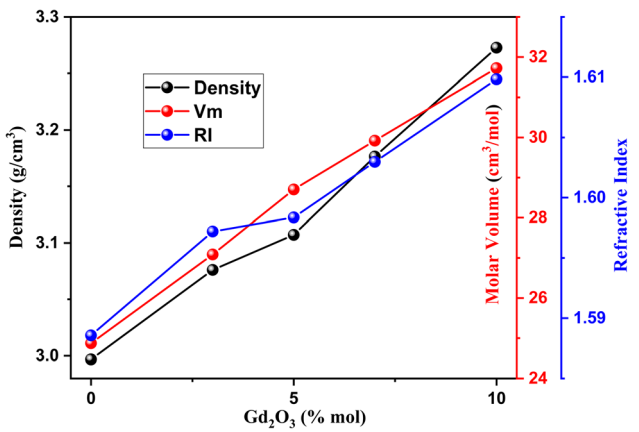

Fig. 4 Physical parameters of LSBNd_*x*Gd glasses *vs.* the Gd_2O_3 content.

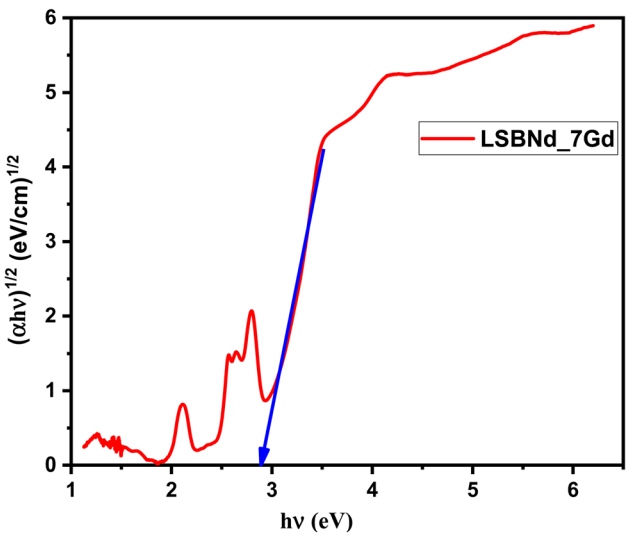

Fig. 6 Tauc's plot for the LSBNd_7Gd sample.

Table 1 Experimental ($f_{exp} \times 10^{-6}$) and theoretical ($f_{theo} \times 10^{-6}$) oscillator strengths and rms deviation (δ_{rms}) of the samples

Peak positions (λ_p, nm)	Energy (cm^{-1})	LSBNd_7Gd	
		f_{exp}	f_{theo}
527	18 975	1.0190	1.2518
584	17 123	17.3332	17.3361
684	14 619	1.0637	1.2984
784	12 755	3.3917	3.0340
806	12 406	11.6965	11.7759
879	11 376	3.1979	3.1229
δ_{rms}	0.204		

on various absorption bands of the Nd ion, in a similar fashion as reported in ref. 28 and 29. The experimental oscillator strengths f_{exp}, f_{theo}, and the root mean square deviation (δ_{rms}) values were found for the LSBNd_7Gd sample listed in Table 1. The slight mismatch between f_{theo} and f_{exp} validated the J–O theory. In the case of the LSBNd_7Gd sample, f_{theo} and f_{exp} were the highest for the absorption peak observed at 584 nm.

The bond covalency with ligands, asymmetry of the localized neodymium centers, rigidity, and viscosity of the host can be predicted from Ω_λ,[29] where Ω_2 represents the covalency, while Ω_4 and Ω_6 demonstrate the rigidity and viscosity of the host, respectively.[29] Here, the parameter $\Omega_6 = 12.43$ ($\times 10^{-20}$ cm^2) was higher than the other two, suggesting a higher viscosity and lower covalency of the bond between Nd and O in the present glass samples. These parameters were calculated from the mixed electric and magnetic dipole absorption transitions. The parameters Ω_4 and Ω_6, unlike Ω_2, are rarely modified with the covalency;[30] therefore, the comparatively small covalency of the glass sample showed a tendency of high viscosity. Table 2 shows that the present sample also followed the same trend of J–O parameters as for previously reported borate glasses.

3.4. Luminescence and radiative features of LSBNd_7Gd samples

Fig. 7 displays the luminescence spectra of the LSBNd_Gd glass, excited at $\lambda = 584$ nm. There were three emission bands present at 918, 1073, and 1340 nm, regardless of the Nd content. The band at 1073 nm was the most intense and exhibited hypersensitive electric dipole characteristics, as validated by the selection rules allowing the transitions $\Delta S = 0$, $\Delta S \leq 2$, and $\Delta J \leq 2$, while the band at 918 nm had the lowest intensity, indicating less sensitive magnetic dipole properties, as validated by the selection rules disallowing the transition $\Delta J \leq 6$. The second strongest transition was the broad $^4F_{3/2} \rightarrow {}^4I_{13/2}$ transition caused by the magnetic dipole effect. This transition is highly important in optical solids, as it is used in 1.057 μm lasers and is suitable for amplification in optical telecommunications within the E-band and O-band[35] Due to concentration quenching, the emission of Gd_2O_3 started to decrease when the concentration exceeded 7 mol%. This decrease was caused by the interaction between host defects and Nd^{3+} ions, leading to concentration quenching and cross-relaxations. As a result, a non-radiative transition occurred.[36] The process of non-

Table 2 Trend of the J–O parameters ($\times 10^{-20}$ cm^2) for the Nd^{3+}-incorporated glasses and their comparison with those of previously reported borate glasses

Sample	Ω_2	Ω_4	Ω_6	Trend	References
LSBNd_7Gd	4.56	4.64	5.43	$\Omega_6 > \Omega_4 > \Omega_2$	Present sample
Bismuth zinc borate	2.67	3.31	3.98	$\Omega_6 > \Omega_4 > \Omega_2$	31
D glass	3.22	3.84	4.33	$\Omega_6 > \Omega_4 > \Omega_2$	32
NCB	3.74	4.48	5.27	$\Omega_6 > \Omega_4 > \Omega_2$	33
LCB	3.53	4.21	5.04	$\Omega_6 > \Omega_4 > \Omega_2$	34
KCB	4.04	4.62	5.83	$\Omega_6 > \Omega_4 > \Omega_2$	34

radiative energy cross-relaxation and resonance energy transfer significantly impacts the spectral emission profile of Nd^{3+} ions. There are multiple states with small energy differences between the $^4F_{3/2}$ and ^4I_J levels, facilitating efficient non-radiative transfer and intense quenching. Resonant energy transfer and non-radiative energy transfer can both contribute to radiative transition and relaxation.[37] The transition from $^2F_{3/2}$ to $^4I_{11/2}$, which occurs at a high intensity at 1073 nm, makes these samples promising for laser applications.

The spectral parameters, such as total radiative transition probability (A_T), gain bandwidth, optical gain, and branching ratios (β_R), were determined using the procedure mentioned in ref. 25, 28 and 29 and are given in Table 3. As found from the ratio of the area of a luminescence band to the total integrated area under the bands, the measured branching ratios (β_{meas}), an essential parameter, are listed in Table 3. Table 3 shows that the branching ratio (β_R) values obtained from $^4F_{3/2} \rightarrow {}^4I_{11/2}$ transition were comparable to those reported in the literature. Table 3 also indicates that the optical gain ($\sigma_{emi} \times \tau_R$), determining the threshold of laser, had a greater value for $^4F_{3/2} \rightarrow {}^4I_{11/2}$ transition at 1073 nm for the LSBNd_7Gd sample. In terms of the range of frequencies where the optical amplification occurs, the gain bandwidth ($\sigma_{emi} \times \Delta\lambda_{eff}$) for the LSBNd_7Gd was comparable with those for glasses reported in previous studies, and is needed for an NIR laser at nearly 1073 nm, a distinct

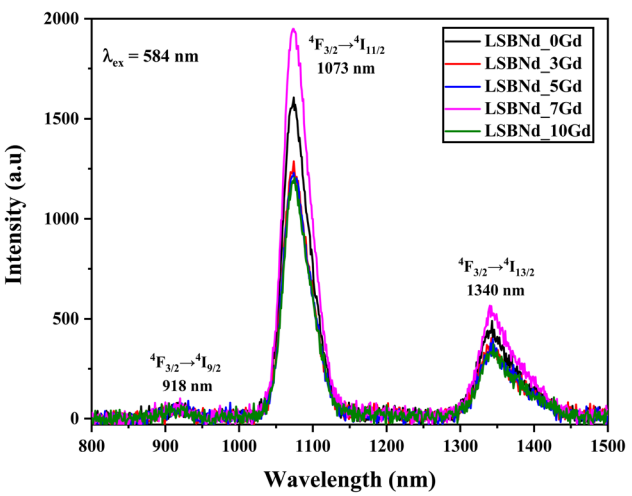

Fig. 7 PL spectra of the samples.

Table 3 Comparison of the radiative transition probability (A_R), radiative branching ratio (β_R), experimental branching ratio (β_{exp}), total radiative transition probability (A_T, s^{-1}), effective bandwidth ($\Delta\lambda_{eff}$), stimulated emission cross-section (σ_{emi}), gain bandwidth ($\sigma_{emi} \times \Delta\lambda_{eff}$), and optical gain ($\sigma_{emi} \times \tau_R$) for the samples with those reported in the literature for similar glass systems

Titled glass	$\Delta\lambda_{eff}$, nm	σ_{emi} (10^{-20} cm^2)	$\sigma_{emi} \times \Delta\lambda_{eff}$ ($\times 10^{-27}$ cm^3)	A_T (s^{-1})	$\sigma_{emi} \times \tau_R$ ($\times 10^{-25}$ cm^2 S)	β_R	β_{meas}	References
ZnAlBiB	30	3.67	1.1	2136	—	72	50	39
BiZNd	37	3.36	1.24	5920	27.9	48	62	40
BNaNf	18	4.18	0.73	—	63.11	38	41	41
BSGdCaNd0.5	32.87	1.39	45.73	750	—	45	58	16
NaF–Na_2O–B_2O_3	57.2	5.0	28.60	—	—	43	—	42
LSBNd_7Gd	28	5.56	1.56	5858	19.71	56	58	Present sample

wavelength for laser applications.[38] These values for $^4F_{3/2} \rightarrow {}^4I_{11/2}$ transition in the studied glasses are comparable [Table 3].

For the $^4F_{3/2} \rightarrow {}^4I_{11/2}$ transition of the studied glasses, the lasing parameters are better than those of other studied systems, as is evident form Table 3. LSBNd_7Gd is thus considered a beneficial sample for realizing broadband optical amplification at 1073 nm.

3.5. Lifetime profiles evaluation

Fig. 8 shows the lifetime profiles at 584 nm excitation and 1073 nm emission for all the samples. The lifetime measured (τ_{exp}) and fitted monoexponentially dropped from 164 μs to 35 μs with elevating the Gd_2O_3 content (Table 4). This shows that the reduction in τ_{exp} was caused by non-radiative relaxation and concentration quenching. From the decay profile, it could be noted that the LSBNd_7Gd glass had a longer experimental lifetime than the other samples. This was because the highest luminescent intensity reduces slowly due to the slow energy transfer to the luminescent center. At this particular concentration, *i.e.*, 7 mol% Gd^{3+}, as a glass structure modifier and sensitizer, the addition prevents the activator's (Nd^{3+}) clustering and, hence, its quick decay.[43] A similar trend has also been observed in the literature.[44]

The mismatch between the experimental and radiative lifetimes, as shown in Table 4, was due to the energy transfer

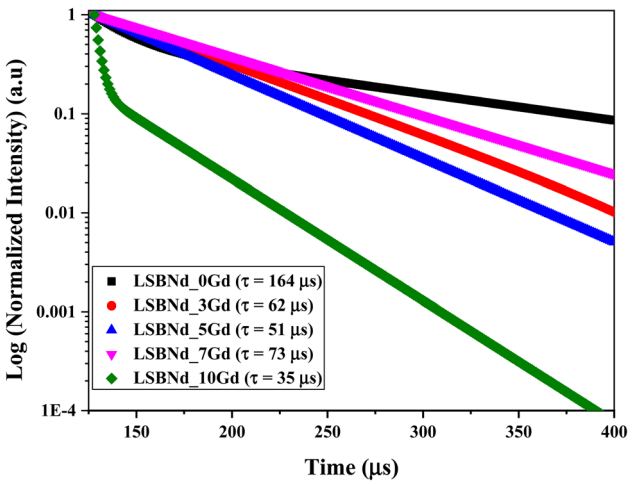

Fig. 8 Decay lifetime of the LSBNd_*x*Gd samples at $\lambda_{exc} = 584$ nm and $\lambda_{emi} = 1073$ nm.

Table 4 Measured (τ_{mes}, μs) and radiative (τ_{rad}, μs) lifetimes, non-radiative decay probability (W_{NR}, s^{-1}), and quantum efficiency (η, %) of various glass systems

Coded glass	τ_{mes}	τ_{rad}	W_{NR}	η	References
BNaNf	151	347	3740	43	46
BBaAZNd0.5	58	244	13 149	24	47
SLBNd1.5	64	155	—	41	48
LSBNd_7Gd	73	170	788	42	Present sample

occurring non-radiatively (NR), which increased with elevating the Gd^{3+} content.[45]

The total luminescence quantum efficiency (η) is given by eqn (1):

$$\eta = \frac{\tau_{mes}}{\tau_{rad}} \quad (1)$$

while eqn (2) gives the NR decay probability (W_{NR}).

$$\frac{1}{\tau_{mes}} = W_{NR} + W_R \quad (2)$$

Table 4 depicts that for the LSBNd_7Gd sample, the non-radiative decay probability was the smallest with an efficient luminescence quantum efficiency. This was due to the ET *via* cross-relaxations, concentration quenching, multi-phonon relaxation, and ET to the luminescence quenching centers.

To study the nature of the interaction mechanism of the Gd fluorescence time, the lifetime curves for 5, 7, and 10 mol% were fitted by the Inokuti–Hirayama (IH) model using eqn (3). A best fit was confirmed for the $S = 6$ dipole–dipole interaction at high Gd concentrations; however, large deviations were shown at low contents.

The ET parameter (Q) of Nd^{3+} is given by eqn (3):

$$Q = \frac{4\pi}{3} \Gamma\left(1 - \frac{3}{S}\right) N_C R^3 \quad (3)$$

where R is the critical separation, Γ is the gamma function and N_c is the acceptors concentration. Dipole–dipole interactions were employed to obtain a good agreement between the experimental and theoretical curves (not shown).

The enhancement in the ET parameter value, *i.e.*, Q, with the elevating dopant concentration, as shown in Table 5, reinforced the dipole–dipole interaction phenomenon among the dopant ions.

Eqn (4) gives the relationship between the interaction parameters C_{DA} and R of Nd^{3+}.

$$C_{DA} = R^{s}\tau^{-1} \quad (4)$$

As shown in Table 5, the C_{DA} increased with increasing the dopant content.

Table 5 shows the parameters Q, R, and C_{DA} as functions of the dopant's concentration, which are more promising than those studied for other borate systems.

3.6. Energy transfer features

Radiative or non-radiative mechanisms are responsible for ET from a donor to an acceptor. Inorganic systems usually have a small absorption strength for the donor, where radiative transfer mostly does not take place,[49] while its occurrence is further lessened due to the low-absorption cross-section of neodymium ions. Two resonance mechanisms cause strong non-radiative energy transfer: the Dexter mechanism (electron exchange) and the Förster mechanism (coulombic interaction).[50,51] The former is prominent when the donor–acceptor separation ranges from 1–10 nm, while at a distance between the donor and acceptor of less than 1 nm, the latter becomes significant.[52] The molar concentration of the dopants in the matrix and density can be utilized by using eqn (5) to estimate the lower limit of their separation:

$$R = \left(\frac{M_m}{\rho N_A x}\right) \quad (5)$$

where R is the donor (Gd) and acceptor (Nd) inter-separation, M_m and ρ are the molar mass and density of the sample, respectively, x is the mol% of the dopant, and N_A is the Avogadro constant.

The calculated R (2.46, 2.12, 1.92, and 1.74 nm) decreased with the addition of the dopant (Gd_2O_3) at 3, 5, 7, and 10 mol%, respectively, confirming that the dominant ET mechanism from Gd to Nd was coulombic interaction in all the samples. The estimated inter Gd and Nd separations could be higher in the presence of Nd agglomerations in the glass; however, the dominancy of the coulombic interaction mechanism would still preserve. The Nd clustering can be minimized by optimizing the dopant concentration and glass-melting conditions.

Fig. 9 illustrates PL spectra of the LSBNd_xGd sample at λ_{exc} = 275 nm, where a gradual decrease could be noticed in the luminescence intensities (312 nm) of the emission spectra, due to the ET from Gd_2O_3 to Nd_2O_3. The peak observed at 625 nm corresponded to the second-order fluorescence in the monochromator, as detailed in ref. 53.

The ET, shown in the energy-level diagram of Fig. 10, takes place by the overlap of the donor emission and acceptor absorption cross-sections.[54] The Gd was raised from the $^8S_{7/2}$ to ^6I_J level upon getting the energy. The Gd de-excites radiatively, giving emission at 312 nm while partly non-radiatively transferring energy to the $^4F_{9/2}$ state of Nd. The ET occurs from Gd^{3+} to Nd^{3+} through the $^6P_{7/2} \rightarrow {}^8S_{7/2}$ transition of Gd. The Nd ions are excited to the $^4F_{9/2}$ state and thereafter relax by making transitions to the ground state ($^4I_{9/2}$), giving typical emissions at 918, 1073, and 1340 nm.

The probability of releasing phonons for the Gd^{3+} (^6P_j) → Nd^{3+} ($^4F_{9/2}$) process is much higher than that in capturing phonons for the Nd^{3+} ($^4F_{9/2}$) → Gd^{3+}(^6P_j) process, because the $^4F_{3/2}$ state (activator) is lower than the ^6P_j states (sensitizer), thus, ET population of the $^4F_{9/2}$ state is enriched. The enhancement of the population due to the addition of Gd^{3+} leads to the sensitization of Nd^{3+} luminescence and results in triggering the excitation of the Nd^{3+} emission.

The ET from Gd to Nd was also analyzed from the lifetime of the LSBNd_xGd at λ_{exc} = 275 nm and λ_{emi} = 312 nm, which was reinforced by a single exponential decay, as illustrated in Fig. 11 and Table 6.

The $\eta_{\tau r}$ listed in Table 6 from the lifetimes of the gadolinium donor and Nd^{3+} acceptor were determined by eqn (6):[17]

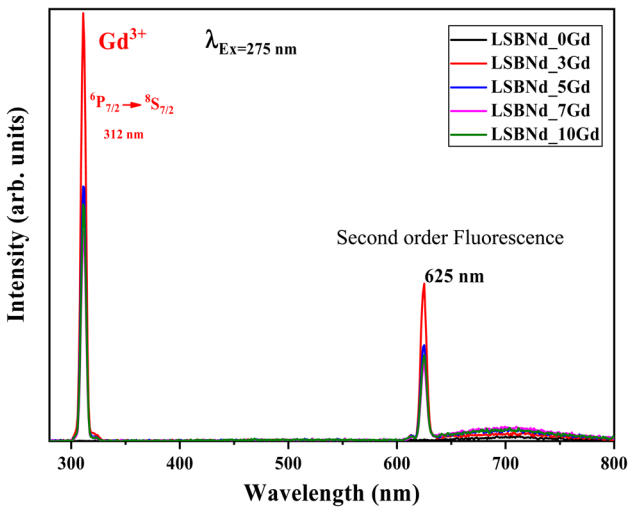

Fig. 9 PL spectra of the LSBNd_xGd samples at λ_{exc} = 275 nm.

Table 5 Comparison of the concentration (N_o, $\times 10^{20}$ ions per cm^3), ET parameter (Q), critical separation (R, Å), and r ($\times 10^{-40}$ cm^6 s^{-1}) for LSBNd_xGd glasses with those reported for other Nd^{3+}-doped borate systems

mol%	N_o	Q	R (Å)	C_{DA} ($\times 10^{-40}$ cm^6 S^{-1})	Ref.
BZBNd10	—	1.85	8.62	37.0	32
BSGdCaNd0.5	1.721	0.43	7.07	3.22	16
LSBNd_5Gd	9.78	0.10	2.44	0.034	Present work
LSBNd_7Gd	13.19	0.16	2.55	0.054	Present work
LSBNd_10Gd	17.87	1.88	5.21	5.752	Present work

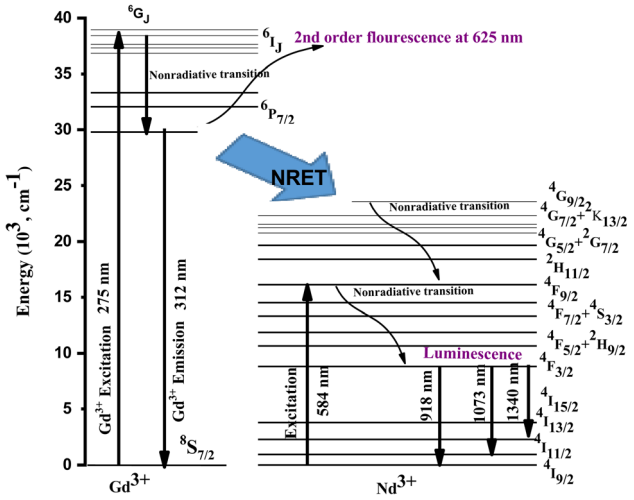

Fig. 10 Energy-levels diagram for the LSBNd_*x*Gd glasses.

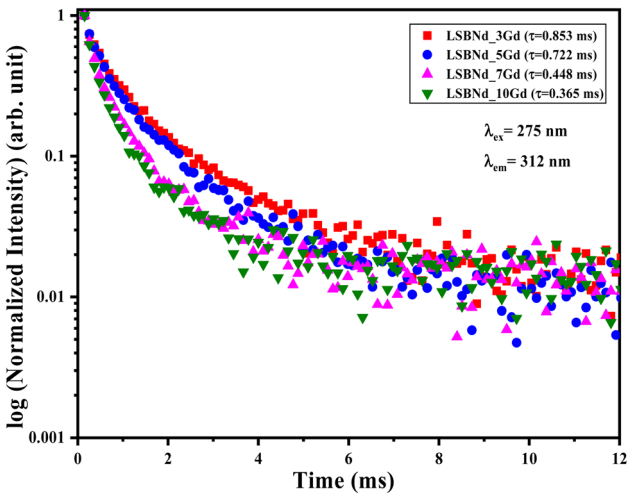

Fig. 11 Decay plots of gadolinium in LSBNd_*x*Gd glasses at λ_{exc} = 275 nm and λ_{emi} = 312 nm.

$$\eta_{tr} = 1 - \frac{\tau_{Gd/Nd}}{\tau_{Gd}} \quad (6)$$

where η_{tr} is the energy transfer efficiency from the donor (Gd) to the acceptor (Nd), and τ_{Gd} and $\tau_{Gd/Nd}$ are the lifetimes of Gd at λ_{exc} = 275 nm and λ_{emi} = 312 nm and Nd at λ_{exc} = 584 nm and λ_{emi} = 1073 nm.

An increase in ET efficiency was expected with the elevating content of Gd_2O_3 from 3% to 10% as the transfer rate increases with the decrease in Gd^{3+}–Nd^{3+} separation. The proximity of the Nd^{3+} acceptor meant the sample contained a significant number of Gd donors, thus increasing the η_{tr}. The ET efficiency increased gradually with the addition of Gd_2O_3 content. An acceptable explanation for this is the non-radiative luminescence quenching of the Gd *via* ET to the Nd.

Table 6 Lifetime (ms) of the dopants (Nd^{3+} and Gd^{3+}) and η_{tr} from Gd to Nd

Glass composition	τ_{Gd} (ms)	τ_{Nd} (ms)	η_{Gd-Nd}
LSBNd_0Gd	—	0.164	—
LSBNd_3Gd	0.853	0.062	0.072
LSBNd_5Gd	0.722	0.051	0.070
LSBNd_7Gd	0.448	0.073	0.162
LSBNd_10Gd	0.365	0.035	0.095

4. Conclusion

By using the typical melt-quenching route, LSBNd_*x*Gd glasses doped with various Gd^{3+} ions contents were developed. The host matrix modification by doping was confirmed from analysis of the physical parameters as well as the XRD and FT-IR spectra. As determined from the absorption spectra, the J–O parameters ($\Omega_2 = 4.56$, $\Omega_4 = 4.64$, $\Omega_6 = 5.43$) were used for calculation of the radiative and laser parameters of Nd^{3+}. Among the three bands in the emission spectra at λ_{exc} = 582 nm, the $^2F_{3/2} \rightarrow {}^4I_{11/2}$ (λ_{em} = 1073 nm) transition was the most intense for all the glass samples and caused the distinctive NIR emission. The determined high stimulated emission cross-sections (5.56×10^{-20} cm^2), branching ratios (56%), and quantum efficiencies (42%) for the $^2F_{3/2} \rightarrow {}^4I_{11/2}$ transition make the LSBNd_*x*Gd glasses favorable for NIR lasers. The lifetimes of Gd ($^6P_{7/2}$ state) and Nd ($^2F_{3/2}$) decreased (from 0.853 to 0.365 ms and 0.164 to 0.035 ms, respectively) with the increase in the dopant ion concentration from 0 to 10 mol%. Gd^{3+} and Nd^{3+} containing optical glasses exhibited prominent NIR (λ_{em} = 1073 nm) and weak 312 nm emissions, proving the $Gd^{3+} \rightarrow Nd^{3+}$ ET. Moreover, while analyzing the ET to the luminescent center, the phonon-assisted non-radiative dipole–dipole interaction was verified as an effective mechanism. Based on the obtained results, the LSBNd_*x*Gd glass with 07 mol% Gd_2O_3 content was found to be optimum for the development of NIR lasers.

Author contributions

I. Ullah: formal analysis, investigation, methodology, writing – original draft, writing – review & editing. C. Sumarah and A. Angnanon: sample preparation and characterization, data curation, methodology, S. A. Khattak: writing – review & editing. S. K. Shah supervision, G. Rooh: investigation, methodology, project administration, software, supervision. I. Khan, M. Shoaib and S. Mukamil: investigation, methodology. S. M. Wabaidur: resources, J. Kaewkhao and S. Kothan: conceptualization, project administration, funding acquisition, resources, software, supervision, validation.

Conflicts of interest

There are no conflicts to declare.

Acknowledgements

The authors wish to acknowledge the Centre of Excellence in Glass Technology and Material Science, Nakhon Pathom Rajabhat University, for providing experimental facilities. Acknowledgment is also made to Thailand Science Research

and Innovation (TSRI) for partially supporting this research. This research was partially supported by Chiang Mai University. CMU Proactive Researcher. Chiang Mai University [Grant number 805/2566]. This research has received funding support from the NRSF *via* the Program Management Unit for Human Resources and Institutional Development, Research and Innovation [grant number B41G670028].

References

1 J.-C. G. Bünzli, S. Comby, A.-S. Chauvin and C. D. Vandevyver, New opportunities for lanthanide luminescence, *J. Rare Earths*, 2007, **25**(3), 257–274.
2 J.-C. G. Bünzli and S. V. Eliseeva, Lanthanide NIR luminescence for telecommunications, bioanalyses and solar energy conversion, *J. Rare Earths*, 2010, **28**(6), 824–842.
3 G. Neelima, K. V. Krishnaiah, N. Ravi, K. Suresh, K. Tyagarajan and T. J. Prasad, Investigation of optical and spectroscopic properties of neodymium doped oxyfluorotitania-phosphate glasses for laser applications, *Scr. Mater.*, 2019, **162**, 246–250.
4 M. Deepa, R. Doddoji, C. D. Viswanath and A. Chandrasekhar, Optical and NIR luminescence spectral studies: Nd^{3+}-doped borosilicate glasses, *J. Lumin.*, 2019, **213**, 191–196.
5 L. Yao, Q. Shao, X. Xu, Y. Dong, C. Liang, J. He, *et al.*, Broadband emission of single-phase $Ca_3Sc_2Si_3O_{12}$: Cr^{3+}/Ln^{3+} (Ln= Nd, Yb, Ce) phosphors for novel solid-state light sources with visible to near-infrared light output, *Ceram. Int.*, 2019, **45**(11), 14249–14255.
6 H. Lin, D. Yang, G. Liu, T. Ma, B. Zhai, Q. An, *et al.*, Optical absorption and photoluminescence in Sm^{3+}-and Eu^{3+}-doped rare-earth borate glasses, *J. Lumin.*, 2005, **113**(1–2), 121–128.
7 K. Bodišová, R. Klement, D. Galusek, V. Pouchlý, D. Drdlík and K. Maca, Luminescent rare-earth-doped transparent alumina ceramics, *J. Eur. Ceram. Soc.*, 2016, **36**(12), 2975–2980.
8 G. Vázquez, I. Camarillo, C. Falcony, U. Caldiño and A. Lira, Spectroscopic analysis of a novel Nd^{3+}-activated barium borate glass for broadband laser amplification, *Opt. Mater.*, 2015, **46**, 97–103.
9 N. Deopa, A. Rao, M. Gupta and G. V. Prakash, Spectroscopic investigations of Nd^{3+} doped lithium lead alumino borate glasses for 1.06 μm laser applications, *Opt. Mater.*, 2018, **75**, 127–134.
10 P. Manasa, D. Ramachari, J. Kaewkhao, P. Meejitpaisan, E. Kaewnuam, A. Joshi, *et al.*, Studies of radiative and mechanical properties of Nd^{3+}-doped lead fluorosilicate glasses for broadband amplification in a chirped pulse amplification based high power laser system, *J. Lumin.*, 2017, **188**, 558–566.
11 R. Balakrishnaiah, P. Babu, C. Jayasankar, A. Joshi, A. Speghini and M. Bettinelli, Optical and luminescence properties of Nd^{3+} ions in K–Ba–Al-phosphate and fluorophosphate glasses, *J. Phys.: Condens. Matter*, 2005, **18**(1), 165.
12 E. A. Lalla, U. Rodríguez-Mendoza, A. Lozano-Gorrín, A. Sanz-Arranz, F. Rull and V. Lavín, Nd^{3+}-doped TeO_2–PbF_2–AlF_3 glasses for laser applications, *Opt. Mater.*, 2016, **51**, 35–41.
13 B. Karthikeyan, S. Mohan and M. Baesso, Spectroscopic and glass transition studies on Nd^{3+}-doped sodium zincborate glasses, *Phys. B*, 2003, **337**(1–4), 249–254.
14 A. Bajaj, A. Khanna, B. Chen, J. G. Longstaffe, U.-W. Zwanziger, J. Zwanziger, *et al.*, Structural investigation of bismuth borate glasses and crystalline phases, *J. Non-Cryst. Solids*, 2009, **355**(1), 45–53.
15 D. R. Rao, G. S. Baskaran, Y. Gandhi and N. Veeraiah, Influence of sesquioxides on luminescence features of Nd^{3+} ions in PbO–PbF_2–B_2O_3 glass system, *Phys. B*, 2015, **457**, 117–125.
16 C. Kesavulu, H. Kim, S. Lee, J. Kaewkhao, N. Wantana, E. Kaewnuam, *et al.*, Spectroscopic investigations of Nd^{3+} doped gadolinium calcium silica borate glasses for the NIR emission at 1059 nm, *J. Alloys Compd.*, 2017, **695**, 590–598.
17 I. Ullah, G. Rooh, S. Khattak, I. Khan, M. Shoaib, S. Kothan, *et al.*, Spectral characteristics and energy transfer in Gd^{3+} and Nd^{3+} doped borate glasses for NIR laser applications, *Infrared Phys. Technol.*, 2022, **125**, 104272.
18 D. Ramteke and R. Gedam, Luminescence properties of Gd^{3+} containing glasses for ultra-violet (UV) light, *J. Rare Earths*, 2014, **32**(5), 389–393.
19 K. Nanda, N. Berwal, R. Kundu, R. Punia and N. Kishore, Effect of doping of Nd^{3+} ions in BaO–TeO_2–B_2O_3 glasses: A vibrational and optical study, *J. Mol. Struct.*, 2015, **1088**, 147–154.
20 P. Pascuta, R. Lungu and I. Ardelean, FTIR and Raman spectroscopic investigation of some strontium–borate glasses doped with iron ions, *J. Mater. Sci.: Mater. Electron.*, 2010, **21**, 548–553.
21 N. Bobkova and S. Khot'ko, Structure of zinc-borate low-melting glasses derived from IR spectroscopy data, *J. Appl. Spectrosc.*, 2005, **72**, 853–857.
22 I. Ullah, C. Sarumaha, A. Angnanon, I. Khan, M. Shoaib, S. Kothan, *et al.*, Effect of Gd_2O_3 concentration on photo and X-rays excited luminescence characteristics of Dy^{3+}-Activated Li_2O_3–SrO–B_2O_3 glass, *Opt. Mater.*, 2022, **133**, 113044.
23 I. Ullah, C. Sarumaha, A. Angnanon, I. Khan, M. Shoaib, S. Khattak, *et al.*, Spectral features of Gd_2O_3 modified Sm^{3+} doped lithium strontium borate glasses for solid-state laser applications, *Ceram. Int.*, 2022, **49**(9), 13774–13782.
24 C. K. Jørgensen and B. Judd, Hypersensitive pseudoquadrupole transitions in lanthanides, *Mol. Phys.*, 1964, **8**(3), 281–290.
25 W. T. Carnall, The absorption and fluorescence spectra of rare earth ions in solution, *Handbook on the Physics and Chemistry of Rare Earths*, 1979, vol. 3, pp. 171–208.
26 J. Tauc, Optical properties of non-crystalline solids, *Opt. Prop. Solids*, 1972, 277–313.
27 N. F. Mott and E. A. Davis, *Electronic Processes in Non-crystalline Materials*, Oxford university press, 2012.

28 B. R. Judd, Optical absorption intensities of rare-earth ions, *Phys. Rev.*, 1962, **127**(3), 750.
29 G. Ofelt, Intensities of crystal spectra of rare-earth ions, *J. Chem. Phys.*, 1962, **37**(3), 511–520.
30 I. I. Kindrat, B. V. Padlyak, R. Lisiecki and V. T. Adamiv, Spectroscopic and luminescent properties of the lithium tetraborate glass co-doped with Nd and Ag, *J. Alloys Compd.*, 2021, **853**, 157321.
31 K. V. Kumar and A. S. Kumar, Spectroscopic properties of Nd^{3+} doped borate glasses, *Opt. Mater.*, 2012, **35**(1), 12–17.
32 B. Shanmugavelu, V. Venkatramu and V. R. K. Kumar, Optical properties of Nd^{3+} doped bismuth zinc borate glasses, *Spectrochim. Acta, Part A*, 2014, **122**, 422–427.
33 Y. Chen, Y. Huang, M. Huang, R. Chen and Z. Luo, Effect of Nd^{3+} on the spectroscopic properties of bismuth borate glasses, *J. Am. Ceram. Soc.*, 2005, **88**(1), 19–23.
34 S. Mohan and K. S. Thind, Investigation of luminescence and spectroscopic properties of Nd^{3+} ions in cadmium alkali borate glasses, *Opt. Mater.*, 2016, **57**, 134–139.
35 E. Kaewnuam, N. Wantana, N. X. Tu, P. H. Minh, K. Yamanoi and J. Kaewkhao, The study on BWGd: Nd glass for new laser amplifier: Properties, theoretical and practical investigations, *Opt. Mater.*, 2022, **129**, 112535.
36 F. Zaman, N. Srisittipokakun, G. Rooh, S. Khattak, N. Singkiburin, H. Kim, *et al.*, Investigation of Li_2O–Gd_2O_3–MO–B_2O_3–Nd_2O_3 (MO= Ba/Bi) glasses for laser applications by Judd–Oflet (J–O) theory, *J. Lumin.*, 2019, **215**, 116639.
37 al. RSNe, *Spectrochim. Acta, Part A*, 2017, **193–197**, 180.
38 J. Rajagukguk, R. Situmorang, M. Djamal, R. Rajaramakrishna, J. Kaewkhao and P. H. Minh, Structural, spectroscopic and optical gain of Nd^{3+} doped fluorophosphate glasses for solid state laser application, *J. Lumin.*, 2019, **216**, 116738.
39 S. Mahamuda, K. Swapna, A. S. Rao, M. Jayasimhadri, T. Sasikala, K. Pavani, *et al.*, Spectroscopic properties and luminescence behavior of Nd^{3+} doped zinc alumino bismuth borate glasses, *J. Phys. Chem. Solids*, 2013, **74**(9), 1308–1315.
40 G. Gupta, A. D. Sontakke, P. Karmakar, K. Biswas, S. Balaji, R. Saha, *et al.*, Influence of bismuth on structural, elastic and spectroscopic properties of Nd^{3+} doped Zinc–Boro-Bismuthate glasses, *J. Lumin.*, 2014, **149**, 163–169.
41 R. Karunakaran, K. Marimuthu, S. Arumugam, S. S. Babu, S. Leon-Luis and C. Jayasankar, Structural, optical absorption and luminescence properties of Nd^{3+} ions in NaO-NaF borate glasses, *Opt. Mater.*, 2010, **32**(9), 1035–1041.
42 B. Karthikeyan and S. Mohan, Spectroscopic and glass transition investigations on Nd^{3+}-doped NaF–Na_2O–B_2O_3 glasses, *Mater. Res. Bull.*, 2004, **39**(10), 1507–1515.
43 T. Suzuki, H. Nasu, M. Hughes, S. Mizuno, K. Hasegawa, H. Ito, *et al.*, Quantum efficiency measurements on Nd-doped glasses for solar pumped lasers, *J. Non-Cryst. Solids*, 2010, **356**(44–49), 2344–2349.
44 B. He, K. Yang, L. Chen, Y. Hua, F. Huang, J. Zhang, *et al.*, Effect of Gd_2O_3 on luminescence properties of RE ions in germanium-tellurite glasses, *J. Lumin.*, 2020, **220**, 116977.
45 I. Kindrat, B. Padlyak and R. Lisiecki, Judd–Ofelt analysis and radiative properties of the Sm^{3+} centres in $Li_2B_4O_7$, CaB_4O_7, and $LiCaBO_3$ glasses, *Opt. Mater.*, 2015, **49**, 241–248.
46 R. Rajaramakrishna, Y. Ruangtawee and J. Kaewkhao, Sm^{3+}-doped molybdenum gadolinium borate glasses for orange emission laser active medium, *Ukr. J. Phys.*, 2018, **63**(8), 720–731.
47 S. S. Babu, C. Jayasankar, P. Babu, T. Tröster, W. Sievers and G. Wortmann, Luminescence and energy transfer properties of Sm^{3+}: borate glasses, *Eur. J. Glasses Sci. Technol. B Phys. Chem. Glasses*, 2006, **47**(4), 548–552.
48 G. Lakshminarayana, A. Meza-Rocha, O. Soriano-Romero, E. Huerta, U. Caldino, A. Lira, *et al.*, Analysis of fluorescence characteristics of Sm^{3+}-doped B_2O_3-rich glasses for Orange-light-emitting diodes, *J. Alloys Compd.*, 2021, **884**, 161076.
49 M. Hughes, H. Li, R. Curry, T. Suzuki and Y. Ohishi, Energy transfer in Cr and Nd co-doped Si-B-Na-Al-Ca-Zr-O glasses, *J. Non-Cryst. Solids*, 2020, **530**, 119769.
50 D. L. Dexter, A theory of sensitized luminescence in solids, *J. Chem. Phys.*, 1953, (21), 836–850.
51 T. Förster, Mechanisms of energy transfer, *Comprehensive biochemistry*, 1967, pp. 61–80.
52 N. Hildebrandt and I. L. Medintz, *FRET-forster Resonance Energy Transfer: from Theory to Applications*, Wiley-VCH Verlag GmbH, 2014.
53 R. A. Buchanan and C. Bueno, Terbium Activated Silicate Luminescent Glasses, *US Pat.*, US5122671A, 1992.
54 Y. Zheng, B. Chen, H. Zhong, J. Sun, L. Cheng, X. Li, *et al.*, Optical transition, excitation state absorption, and energy transfer study of Er^{3+}, Nd^{3+} single-doped, and Er^{3+}/Nd^{3+} codoped tellurite glasses for mid-infrared laser applications, *J. Am. Ceram. Soc.*, 2011, **94**(6), 1766–1772.